Metal-Organic Redox Vehicles to Encapsulate Organic Dyes for Photocatalytic Proton and Carbon Dioxide Reduction

Journal:	*Inorganic Chemistry Frontiers*
Manuscript ID	QI-RES-06-2016-000211.R1
Article Type:	Research article
Date Submitted by the Author:	03-Aug-2016
Complete List of Authors:	Yu, Hao; Dalian University of Technology, State Key Laboratory of Fine Chemicals He, Cheng; Dalian University of Technology, State Key Laboratory of Fine Chemicals Jing, Xu; Dalian University of Technology, State Key Laboratory of Fine Chemicals Duan, Chunying; Dalian University of Technology, State Key Laboratory of Fine Chemicals Reek, J; van 't Hoff Institute for molecular sciences,

Journal Name

ARTICLE

Metal-Organic Redox Vehicles to Encapsulate Organic Dyes for Photocatalytic Proton and Carbon Dioxide Reduction

Received 00th January 20xx,
Accepted 00th January 20xx

DOI: 10.1039/x0xx00000x

www.rsc.org/

Hao Yu,[a] Cheng He,[a]*Jing Xu,[a] Chunying Duan[a] and Joost N. H. Reek[b]

The application of metal-organic molecular hosts as "molecular flasks" has precipitated a surge of interest in the reactivity and property of molecules within well-defined spaces. Here we report an approach to construct supramolecular systems for photo-catalytic hydrogen production and carbon dioxide reduction by encapsulating an organic dye molecule into the pocket of the redox-active metal-organic macrocycle. The assembled Ni_3L_3 tricycle consists of three ligands and three nickel ions that alternatively connect together. The special geometry enforces the distortion of the square planar coordinated configuration, and the coordination of the sulphur atoms enables the modification of redox potentials suitable for proton reduction and carbon dioxide reduction. The supramolecuar systems that have fluorescein molecules being encapsulated as the photosensitive guests feature efficient activity for the photocatalytic carbon dioxide conversion and production reduction. The new reaction pathways within the confined space demonstrate the power of the supra-molecular system over related systems.

Introduction

The design of artificial catalysts that compete with the catalytic proficiency of enzymes is an intensive subject of research.[1]The typical route to prepare an effective artificial enzyme is to reproduce the sometimes elusive structure of the enzyme's active site[2] and at the same time to enhance the reaction rate by increasing the local concentration of a substrate around its reactive center.[3] In this case, self-assembly reaction vessels based on reversible interactions have been considered a new phase of matter, in which the physicochemical properties of the molecules contained in the "molecular flask" are considerably modified with respect to those exhibited in the solid, liquid, or gas phase.[4] New reaction pathways have also emerged for substrate molecules inside these containers, by enhancing the proximity between the substrate and the catalytic center and increasing the effective molarity of the reaction.[5]

An important target in area of artificial enzyme mimics is the photo-catalytic reduction of chemical protons and carbon dioxide, as it allows to store renewable and abundant energy in chemical bonds. In a final target device coupling the reductive and oxidative half-reactions is required.[6] The homogeneous systems that have been reported to perform such a reductive half reaction require a photosensitizer for light absorption, a catalyst for CO_2 activation, and an artificial electron donor. Such systems offer a nice strategy for solar driven CO_2 fixation that allows for modular tuning of their performances *via* synthetic chemistry.[7] Compared to related heterogeneous catalytic systems[8], the advantage entails the freedom to design molecular components for the homogeneous systems, preferably based on earth-abundant metal catalyst.[9] However, it still remains a challenge to control and optimize the photo-induced electron transfer between the photosensitizer and the catalyst.

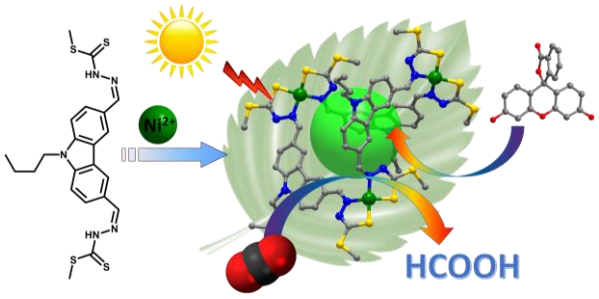

Scheme 1. Procedure for the synthesis of the metal-organic macrocycle and construction of the artificial supramolecular system for photocatalytic carbon dioxide reduction. The nickel, sulfur, nitrogen and carbon were drawn in green, yellow, blue and grey, respectively.

Supramolecular assembly of predesigned inorganic and organic building blocks can be used to construct the well-defined, nanosized molecular cavities that catalyse special chemical transformations.[10] Previously, we have developed the new approach to the creation of artificial photocatalytic

[a]*State Key Laboratory of Fine Chemicals, Dalian University of Technology Dalian, 116012, China. E-mail: hecheng@dlut.edu.cn.*
[b]*Homogeneous and Supramolecular Catalysis Group, Van't Hoff Institute for Molecular Science, University of Amsterdam, Science Park 904, 1098 XH Amsterdam, The Netherlands.*
Electronic Supplementary Information (ESI) available: [details of any supplementary information available should be included here]. See DOI: 10.1039/x0xx00000x

systems for light driven proton reduction by encapsulating organic photosensitizers into the pockets of redox metal-organic macrocycles,[11] thus we considered whether such a strategy could provide a model platform for efficient photo-catalytic proton reduction and carbon dioxide reduction.[12] Herein, by incorporating hydrazinecarbodithioate chelators into the ligand backbone, we extended this approach to assemble metal-organic macrocycles that act as a supramolecular host and redox catalyst for the photo-catalytic reduction of carbon dioxide (**Scheme 1**). Based on seminal work with $[Ni(cyclam)]^{2+}$ and related N_4 macrocyclic complexes that show catalytic activation for the carbon dioxide electro-chemical reduction,[13] we reasoned that the planar, electron-rich systems with a d_z^2 based nucleophile could provide active sites for activating CO_2 as an electrophile.[14] The strong coordinating ability of the NS chelators was expected to enhance the stability of the macrocycle and to afford nickel ions with redox potentials[15] and square plane coordination geometry suitable for carbon dioxide reduction.[16] The special macrocyclic conformation could be also well-defined to provide sufficient intermolecular interactions with organic dye molecules encapsulated for the construction of supramolecular photocatalytic systems.

Experimental

Materials and methods

All chemicals were of reagent grade quality obtained from commercial sources and used without further purification. MeCN was distilled from calcium hydride for use. The elemental analyses of C, H and N were performed on a Vario EL III elemental analyzer. ^{1}H NMR, ^{13}C NMR and NOESY spectra were measured on a Varian INOVA 400 M spectrometer. ESI mass spectra were carried out on a HPLC-Q-Tof MS spectrometer. UV−vis spectra were measured on a HP 8453 spectrometer. The solution fluorescent spectra were measured on JASCO FP−6500. The solution of Ni-**SSC** and Ni-**MSSC** was prepared in DMF, and the concentration was 1.0 mM, whereas the solution of fluorescein was prepared in acetonitrile/H_2O (1:1 v:v).

All electrochemical measurements were carried out under nitrogen atmosphere at room temperature and performed on a CHI 1130 (CH Instrument Co., Shanghai) electrochemical analyzer with a conventional three-electrode system consists of a homemade Ag/AgCl electrode as a reference electrode, a platinum silk with 0.5 mm diameter as a counter electrode, and a glassy carbon electrode as a working electrode. The solution concentrations for electrochemical measurements were *ca.* 0.1 mM for the Ni-**SSC** and 1 mM for the Ni-**MSSC** and 0.1 M for the supporting electrolyte, $(n\text{-}Bu_4N)PF_6$. Electrodes were polished on a MD−Nap polishing pad.

Photoinduced hydrogen evolution and carbon dioxide reduction were carried out in a 20 mL flask. Varying amounts of the catalyst, fluorescein and triethylamine in 1:1 acetonitrile/H_2O (v:v) were added to obtain a total volume of 5.0 mL. The flask was sealed with a septum and degassed by bubbling argon for 30 min and carbon dioxide for 5 min under atmospheric pressure at room temperature. The pH of this solution was adjusted to a specific pH by adding hydrochloric acid and measured with a pH meter. After that, the samples were irradiated by a 500 W Xenon Lamp, and the reaction temperature was remained at 25 °C by a super constant temperature circulating water tank. The generated photoproduct of H_2 was characterized on a GC 7890T instrument equipped with a 5 Å molecular sieve column (0.6 m × 3 mm) and a thermal conductivity detector, and argon was used as carrier gas. The amount of generated hydrogen was determined by the external standard method. Hydrogen in the resulting solution was not measured and the slight effect of the generated hydrogen gas on the pressure of the flask was neglected for calculation of the volume of hydrogen gas.[17] The generated HCOOH was characterized on a DIONEX ICS-5000 instrument using a guard column IonPac AG11-HC and the column temperature was kept at 30 °C. The photocatalytic reduction of $^{13}CO_2$ was carried out in a CH_3CN/D_2O solution (ensuring the same condition as that of the reaction mixture mentioned above for photocatalytic reduction of CO_2). The solution was degassed by bubbling Ar for 30min and $^{13}CO_2$ for 5min. To avoid the influence of residue coordination complexes on the detection of ion chromatography and NMR, the CH_3CN was removed by vacuum rotary evaporation after the reaction. The residual D_2O was filtered to remove the residue complex before the measurement of ^{13}C NMR spectroscopy.

Synthetic procedures

Preparation of Ni-SSC

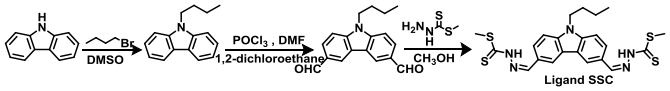

Scheme 2. Synthesis of ligand **SSC**

9-butyl-9*H*-carbazole. A solution of carbazole (5.0 g, 30 mmol) and KOH (3.4 g, 60 mmol) in dimethyl sulfoxide (100 mL) under stirring was heated at 90 °C for 4 h, and then 1-bromobutane (4.1 g, 30 mmol) was gradually added. After being stirred for another 48 h at 90 °C, the mixture was poured into water (100 mL) and extracted with dichloromethane. The organic layer was washed with water (100 mL × 3) and brine (100 mL × 3), and then dried over anhydrous magnesium sulfate. The solvent was removed by vacuum rotary evaporation to obtain a crude product. The residue was purified by silica gel column chromatography (dichloromethane/petroleum ether, 1:1 as an eluent).[18] Yield: 5.9 g, 88%. ^{1}H NMR ($CDCl_3$, 400 MHz, *ppm*): δ 8.00 (d, *J* = 8.0 Hz, 2H carbazole), 7.19-7.48 (m, 6H carbazole), 4.31 (t, *J* = 6.8 Hz, 2H NCH_2), 1.86 (m, 2H CH_2), 1.39 (m, *J* = 7.6 Hz, 2H CH_2), 0.95 (t, *J* = 7.6 Hz, 3H CH_3).

9-butyl-9*H*-carbazole-3,6-dicarbaldehyde. Phosphoryl chloride (23 g, 150 mmol) was added dropwise to a solution of N,N-dimethylformamide (11 g, 150 mmol) in 1,2-dichloroethane (10 mL) at 0 °C. Then the reaction mixture was heated to 35 °C, and a solution of 9-butyl-9*H*-carbazole (3.35 g, 15 mmol) in 1,2-dichloroethane (40 mL) was added. After being stirred for 48 h at 90 °C, the mixture was poured into water (200 mL) and extracted with dichloromethane. The organic layer was washed with water (100 mL × 3) and brine (100 mL × 3), and then dried over anhydrous magnesium sulfate. The solvent was removed by vacuum rotary evaporation. The residue was purified by silica gel column chromatography (dichloromethane/petroleum ether, 4:1 as an

eluent). Yield: 2.1 g, 67%. ^{1}H NMR ($CDCl_3$, 400 MHz, *ppm*): δ 10.13 (s, 2H CHO), 8.67 (s, 2H carbazole), 8.08 (d, *J* = 8.8 Hz, 2H carbazole), 7.55 (d, *J* = 8.4 Hz, 2H carbazole), 4.39 (t, *J* = 6.8 Hz, 2H NCH_2), 1.78 (m, *J* = 7.5 Hz, 2H CH_2), 1.30 (m, *J* = 7.6 Hz, 2H CH_2), 0.88 (t, *J* = 7.6 Hz, 3H CH_3).

Ligand SSC. Methyl hydrazinecarbodithioate (1.47 g, 12 mmol) was added to a methanol solution (50 mL) containing 9-butyl-9*H*-carbazole-3,6-dicarbaldehyde (1.40 g, 5 mmol). After 5 drops of acetic acid was added, the mixture was refluxed for 48 h. The yellow solid was collected by filtration, washed with methanol and dried under vacuum. Yield: 1.8 g, 43%. ^{1}H NMR (DMSO, 400 MHz, *ppm*): δ 13.32 (s, 2H CNH), 8.53 (s, 2H carbazole), 8.46 (s, 2H NCH), 7.94 (d, *J* = 8.8 Hz, 2H carbazole), 7.46 (d, *J* = 8.4 Hz, 2H carbazole), 4.39 (t, *J* = 6.8 Hz, 2H NCH_2), 2.56 (s, 6H SCH_3), 1.78 (m, *J* = 7.5 Hz, 2H CH_2), 1.30 (m, *J* = 7.6 Hz, 2H CH_2), 0.88 (t, *J* = 7.6 Hz, 3H CH_3). Anal. Calc. for $C_{22}H_{25}N_5S_4$: C, 54.18; H, 5.17; N, 14.36; Found: C, 54.03; H, 5.11; N, 14.21.

Ni-**SSC.** A solution of $Ni(ClO_4)_2{\cdot}6H_2O$ (73.1 mg, 0.2 mmol) and ligand **SSC** (48.7 mg, 0.1 mmol) in 40 mL CH_2Cl_2/CH_3OH (1:1 v:v) was stirred at room temperature. After being stirred for 6 h, the reaction solution was poured into 200 mL diethyl ether and filtered, and then the precipitated crude product was dissolved in DMF 30 mL and stirred for 12 h. Black purple rhombus crystals of Ni-**SSC** were obtained by diffusing diethyl ether into the aforementioned DMF solution. Yield: about 65%. Anal. Calc. for $Ni_3(C_{66}H_{69}N_{15}S_{12})$: H, 4.26; C, 48.54; N, 12.86; Found: H, 4.12; C, 46.82; N, 12.14.

Preparation of Ni-MSSC

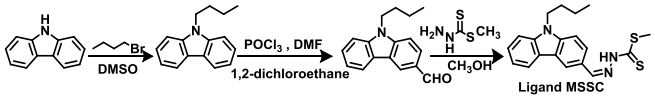

Scheme 3 Synthesis of ligand **MSSC**

9-butyl-9*H*-carbazole-3-carbaldehyde. Phosphoryl chloride (11.5 g, 75 mmol) was added dropwise to a solution of N,N-dimethylformamide (5.5 g, 75 mmol) in 1,2-dichloroethane (10 mL) at 0 °C. Then the reaction mixture was heated to 35 °C, and a solution of 9-butyl-9*H*-carbazole (2.2 g, 10 mmol) in 1,2-dichloroethane (40 mL) was added. After being stirred for 48 h at 90 °C, the mixture was poured into water (200 mL), extracted with dichloromethane, and the organic layer was washed with water (100 mL × 3) and brine (100 mL × 3), and then dried over anhydrous magnesium sulfate. The solvent was removed by vacuum rotary evaporation to give a residue that was purified with silica gel column chromatography afterwards (dichloromethane/petroleum ether, 2:1 as an eluent). Yield: 1.96 g, 78%. ^{1}H NMR (DMSO, 400 MHz, *ppm*): δ 10.13 (s, 1H CHO), 8.45 (s, 1H carbazole), 8.23 (d, *J* = 7.6 Hz, 1H carbazole), 7.90 (d, *J* = 8.8 Hz, 1H carbazole), 7.70 (d, *J* = 8.4 Hz, 1H carbazole), 7.65 (d, *J* = 8.4 Hz, 1H carbazole), 7.50 (t, *J* = 7.8 Hz, 1H carbazole), 7.26 (t, *J* = 7.4 Hz, 1H carbazole), 4.43 (t, *J* = 6.8 Hz, 2H NCH_2), 2.56 (s, 3H SCH_3), 1.77 (m, *J* = 7.5 Hz, 2H CH_2), 1.31 (m, *J* = 7.6 Hz, 2H CH_2), 0.96 (t, *J* = 7.6 Hz, 3H CH_3).

Ligand MSSC. Methyl hydrazinecarbodithioate (0.74 g, 6 mmol) was added to a methanol solution (50 mL) containing 9-benzyl-3-carbaldehydecarbazole (1.26 g, 5 mmol). Subsequently, five drops of acetic acid was added and the mixture was refluxed for 48 h. The yellow solid was collected by filtration, washed with methanol and dried in vacuum. Yield: 1.6 g, 75%. ^{1}H NMR (DMSO, 400 MHz, *ppm*): δ 13.29 (s, 1H CNH), 8.45 (s, 1H carbazole), 8.43 (s, 1H NCH), 8.23 (d, *J* = 7.6 Hz, 1H carbazole), 7.90 (d, *J* = 8.8 Hz, 1H carbazole), 7.70 (d, *J* = 8.4 Hz, 1H carbazole), 7.65 (d, *J* = 8.4 Hz, 1H carbazole), 7.50 (t, *J* = 7.8 Hz, 1H carbazole), 7.26 (t, *J* = 7.4 Hz, 1H carbazole), 4.43 (t, *J* = 6.8 Hz, 2H NCH_2), 2.56 (s, 3H SCH_3), 1.77 (m, *J* = 7.5 Hz, 2H CH_2), 1.31 (m, *J* = 7.6 Hz, 2H CH_2), 0.96 (t, *J* = 7.6 Hz, 3H CH_3). Anal. Calc. for $C_{19}H_{21}N_3S_2$: C, 64.19; H, 5.95; N, 11.82; Found: C, 63.89; H, 5.87; N, 11.56.

Ni-MSSC. A solution of $Ni(OAc)_2{\cdot}4H_2O$ (24.8 mg, 0.1 mmol) and ligand **MSSC** (71.1 mg, 0.2 mmol) in 40 mL CH_2Cl_2/CH_3OH (1:1 v:v) was stirred for 12 h. Dark red solution of Ni-**MSSC** was obtained through filtration and black block crystals were obtained in the above solution by volatilization after one week. Yield: about 68%. Anal. Calc. for $Ni(C_{38}H_{40}N_6S_4)$: H, 5.25; C, 59.45; N, 10.95; Found: H, 5.14; C, 58.95; N, 10.72.

Crystallography.

The diffraction intensities were collected on a Bruker SMART APEX CCD diffractometer equipped with a graphite-monochromated Mo−Kα (λ = 0.71073 Å) radiation source; the data were acquired using the SMART and SAINT programs.[19] The structures were solved by direct methods and refined on F^2 by full-matrix least-squares methods using the SHELXTL version 5.1 software.[20]

Of the refinement of both data, non-hydrogen atoms were refined anisotropically. Except the solvent water molecule, hydrogen atoms were fixed geometrically at calculated distances and allowed to ride on the parent non-hydrogen atoms. For data of Ni-**SSC**, one carbon atom of butyl group was disordered into two parts with the site occupancy factors (s.o.f.) of each parts being refined using free variable, respectively. Several bond distances in the disordered butyl group and the solvent DMF molecules were restrained as idealized values. Thermal parameters on adjacent atoms of the disordered butyl group and the solvent DMF molecules were restrained to be similar. The SQUEEZE function of PLATON was used to remove the void electron density. The level A and B alerts in check cif file are mainly due to the low diffraction intensity of the data.

Crystal data for Ni-SSC. $Ni_3C_{75}H_{92}N_{18}O_4S_{12}$, Mr=1870.52, Triclinic, space group P-1, black block, a = 18.28(2) Å, b = 18.49(2) Å, c = 19.33(2) Å, α = 112.371(12), β = 114.135(11), γ = 95.882(11), V = 5250(11) Å^3, Z = 2, λ (MoKα) = 0.71073 Å, μ (MoKα)= 0.819 mm^{-1}, T = 220(2) K, 18178 unique reflections [R_{int} = 0.1686], Final R_1 [with I > 2σ(I)] = 0.1101, wR_2 (all data)= 0.3986. **CCDC NO. 1450384**.

Crystal data for Ni-MSSC. $NiC_{38}H_{40}N_6S_4$, Mr=767.71, Orthorhombic, space group P2(1)2(1)2(1), black block, a = 8.454(2) Å, b = 18.860(4) Å, c = 23.003(5) Å, V = 3667.7(15) Å^3, Z = 4, λ (MoKα) = 0.71073 Å, μ (MoKα)= 0.794 mm^{-1}, T = 220(2) K, 6452 unique reflections [R_{int} = 0.0854], Final R_1 [with I > 2σ(I)] = 0.0556, wR_2 (all data) = 0.1268. **CCDC NO. 1450385**.

Results and discussion

Ligand **SSC** was obtained by a simple Schiff-base reaction of 9-butyl-3,6-dicarbaldehydecarbazole with methyl hydrazinecarbodithioate in a methanol solution. Vapor diffusion of

diethyl ether into the DMF solution mixed ligand **SSC** and $Ni(ClO_4)_2{\cdot}6H_2O$ in an equal a 1:2 mole ratio led to the formation of crystalline solids of Ni-**SSC** in a yield of about 60%. Single crystal X-ray structural analysis of compound Ni-**SSC** displayed the formation of a three-membered metal-organic macrocycle. The complex consists of three ligands and three nickel ions that connect together alternatively. Each ligand binds to the central Ni ion through the thiol S atom and hydrazine N atom to yield a five-membered chelated ring, and each nickel ion is positioned at the corners of a triangle. The NiN_2S_2 moiety is *cis* square-planar (coordination plane) with Ni-S and Ni-N bond distances of 2.14 Å and 1.92 Å,[21] in accordance with those nickel(II) SN chelating complex.[22] The distance between a pair of nickel ions is about 12.1 Å and the inner radii of the macrocycle is about 4.52 Å. As Ni-**SSC** composes of three ligands and three nickel ions and each ligand has a certain rigidity, the formation of the three membered metal organic macrocycle enforces the distortion of the square-planar NiN_2S_2 moiety with the pairs of sulphur and the nitrogen atoms position at a *cis* configuration. The average dihedral angle between the pair of the chelating planes are 27.9, 25.1 and 19.0°, respectively. Such a structural distortion and the rigidity of the robust ligands further led to the conformation warp of the triangle with a special geometry[16], from which the aromatic groups of the ligands extended outside. This structure is just like a shopping bag, which provides a pocket for encapsulation of guest molecules with aromatic rich groups through π-π stacking interactions between the guest molecules, forming supramolecular systems.

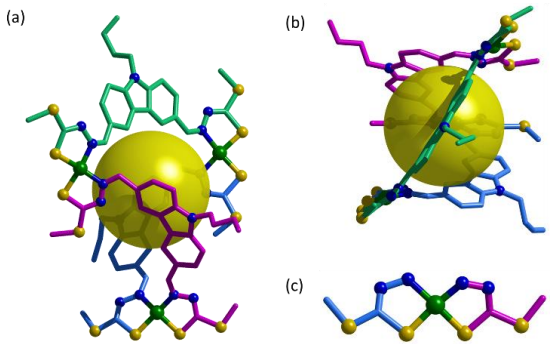

Figure 1. The structure of the molecular triangle Ni-SSC showing at the obverse side (a), the flank side (b) and the coordination geometry of the Ni atom (c). The Ni, S and N atoms are drawn in green, yellow and blue, respectively.

ESI-MS spectrum (Figure 2) of compound Ni-**SSC** in a DMF solution exhibits one intense peak at *m/z* = 1632.08. The peak was assigned to the species of $[Ni_3(\mathbf{SSC})_3H]^+$, suggesting the composition and stability of the nickel macrocycle species in solution. When an equimolar amount of fluorescein (**Fl**) was added into the solution of Ni-**SSC**, a new intense peak at *m/z* = 1966.14 was observed. Analysis of the corresponding isotope patterns reveals that the peak is properly assigned to the $[\mathbf{Fl}{\subset}Ni_3(\mathbf{SSC})_3H]^+$, suggesting the formation of a 1:1 stoichiometric complexation species **Fl**⊂Ni-**SSC** in the solution. UV absorption revealed the presence of interactions between the host ligands and guests (Figure S5), most possibly due to π-π interactions between the aromatic rings of Ni-**SSC** and **Fl**.

Cyclic voltammograms of the macrocycle Ni-**SSC** (0.1 mM) recorded in a DMF solution shows the coupled Ni^{II}/Ni^{I} reduction process (exhibiting a reversible reduction at −0.98 V vs SCE under argon atmosphere, Figure 3a). The potentials fall well within the range of proton reduction in aqueous media.[23] Addition of $\mathbf{Et_3N}H^+$ triggers the appearance of a new cathodic wave near the Ni^{II}/Ni^{I} response. Increasing the concentration of $\mathbf{Et_3N}H^+$ raises the intensity of the new wave and shifts it to more negative potentials. This wave is attributed to the proton reduction process, indicating that Ni-**SSC** is able to reduce the proton in the electrochemical condition.[24] Exposure of Ni-**SSC** to CO_2 also causes the appearance of a catalytic wave at the second reduction process, and addition of excess water as a proton source further enhances the current.[25] However, no current enhancement is observed upon addition of water alone at the same levels, indicating the selectivity for the reduction over protons from water.

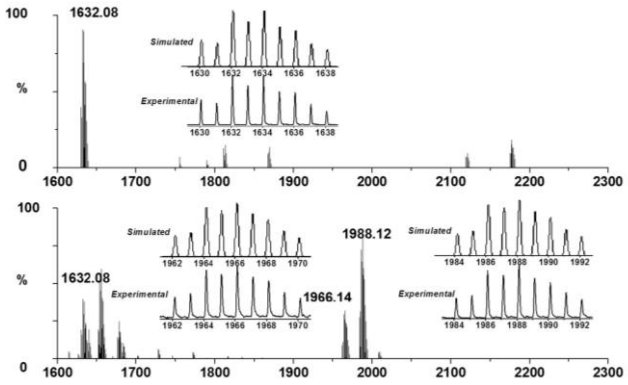

Figure 2. ESI-MS spectra of Ni-**SSC** in a DMF solution (top picture) and of **Fl** in the aforementioned solution (bottom picture). The inserts show the measured and simulated isotopic patterns at *m/z* =1632.08 (top) and *m/z* = 1966.14 (bottom), respectively.

Addition of 15 μM Ni-**SSC** to the solution of **Fl** (10 μM) in a CH_3CN/H_2O solution (ensuring the same condition as that of the reaction mixture mentioned below for photocatalytic reduction of CO_2) quenched approximately 40% of the emission intensity of **Fl**, and the luminescent titration profile of **Fl** in the solution was consistent with the Hill-plot.[26] The best fit of the titration profile suggested a 1:1 host-guest behavior with an association constant calculated as $3.88 \pm 0.02 \times 10^4$ M^{-1} (Figure 3c).The quenching process is probably mainly attributed to a photoinduced electron transfer (PET) from the excited state **Fl*** to the redox Ni centers in Ni-**SSC**,[27] and partly caused by the stacking interaction of **Fl** with the ligands. As a consequence, Ni-**SSC** was directly activated for proton reduction by the excited state **Fl*** during irradiation. Further investigation of the luminescence at 520 nm of a **Fl** solution (10 μM) containing Ni-**SSC** (20 μM) decayed in a clearly exponential fashion with the lifetime, similar to the luminescence of a solution of free **Fl** (4.62 ns).The fact that the luminescence was strongly quenched but the lifetime of the luminescence was maintained suggested that there were two

luminescent species coexisted in the titration mixture: one is the **Fl** species itself with its fluorescent lifetime being maintained; the other is the host-guest complexation species **Fl**⊂Ni-**SSC**, which exhibits ignored luminescent intensity with quite low lifetime. Thus the quenching process from the excited state of **Fl*** to Ni-**SSC** was not a usually bimolecular process, but belong to a fast, pseudo-intramolecular electron transfer process attributable to the host-guest complexation.[12b]

The irradiation of a solution containing **Fl** (4.0 mM), Ni-**SSC** (10.0 μM), and **TEA** (10% v:v) in a CH_3CN/H_2O (1:1 in volume) solution at 25°C resulted in direct hydrogen generation.[28] A higher efficiency of hydrogen production was achieved at pH = 11–12.0 (Figure S13). Control experiments revealed that the absence of any of these individual components led to failure to produce hydrogen, demonstrating that all three species are essential for hydrogen generation. Of course, the artificial system could not function well in the absence of light. When the concentrations of **Fl** (4.0 mM) and **TEA** (10% in volume) were fixed, the volume of the hydrogen production exhibited a linear relationship with the concentration of the Ni-**SSC** catalyst in the range of 10.0 μM to 40.0 μM (Figure 3d). The initial turnover frequency (**TOF**) was approximately 160 moles of hydrogen per mole of catalyst per hour, and the calculated turnover number (**TON**) was approximately 1,250 per mole of catalyst.

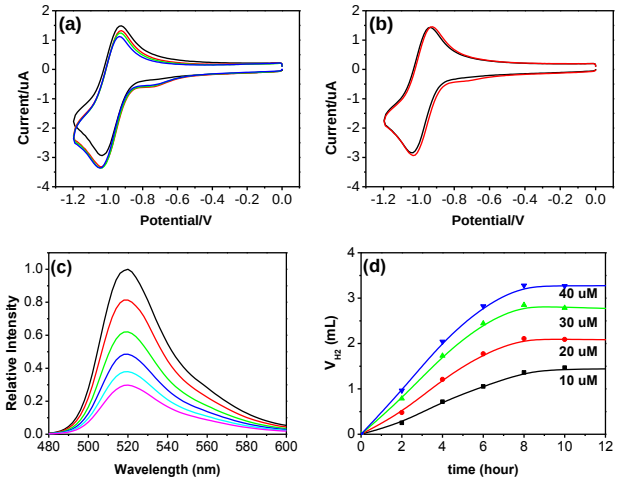

Figure 3. (a) Cyclic voltammograms of 0.1 mM Ni-**SSC** (black line) upon addition of Et_3NH^+ with different concentrations of 2 mM (red line), 4 mM (green line) and 6 mM (blue line); (b) upon exposure to CO_2 up to saturation (red line). Scan Rate: 100 mV/s; (c) Family of luminescence spectra of fluorescein upon the addition of Ni-**SSC** in CH_3CN/H_2O solution, excited at 470 nm and (d) Light-driven hydrogen evolution of the systems containing **Fl** (4.0 mM), **TEA** (10% v/v), and Ni-**SSC** in a CH_3CN/H_2O solution (1:1, pH = 11.0) with the concentration of Ni-**SSC** fixed at 10 μM (black line), 20 μM (red line), 30 μM (green line), and 40 μM (blue line), respectively.

Photocatalytic reduction of CO_2 was then conducted with Et_3N (10.0% in v/v) in 5 mL CH_3CN/H_2O solution under irradiation. The system exhibits obviously photocatalytic activity for CO_2 reduction. The $HCOO^-$ anion was continuously produced, with the amount increasing to 0.46 μmol in 12 h. The initial **TOF** was approximately 0.8 moles of $HCOO^-$ per mole of catalyst per hour, and the calculated **TON** was approximately 9.3 per mole of catalyst. Few H_2 can be detected in the gas and no other products can be detected in liquid phases, suggesting that the catalyst is highly selective toward the CO_2 conversion. No $HCOO^-$ could be detected in the absence of any component of Ni-**SSC,** Et_3N, or **Fl**, demonstrating their critical roles in the reaction. Moreover, no $HCOO^-$ was generated when the reaction was carried out in the dark, suggesting a truly photocatalytic behavior.

To verify the origin of $HCOO^-$, the isotopic $^{13}CO_2$ instead of CO_2 was employed as a reactant to be introduced into the reaction system under otherwise similar conditions, and the product was identified by ^{13}C NMR spectroscopy to confirm the origin of $HCOO^-$.[29] As shown in Figure 4, the ^{13}C NMR spectrum clearly gave a peak at 164.5 ppm, corresponding to $H^{13}COO^-$. The results demonstrate that the produced $HCOO^-$ anion indeed comes from CO_2. From a mechanistic viewpoint, the encapsulation of one molecule of the organic dye **Fl** inside the pocket of the molecular macrocycle Ni-**SSC** first enhances the proximity between the nickel-based redox catalytic site and the photosensitizer **Fl**. This supramolecular structure then allows a direct photo-induced electron transfer (**PET**) process from the excited state **Fl*** to the redox catalyst. Simultaneously, the close proximity between the redox site and the photosensitizer within the confined space further allows the photo-induced electron transfer to occur in a more powerful pseudo-intramolecular pathway to avoid unwanted electron transfer.[30] With the activation upon coordination to the reduced nickel center, carbon dioxide was reduced to $HCOO^-$ directly.

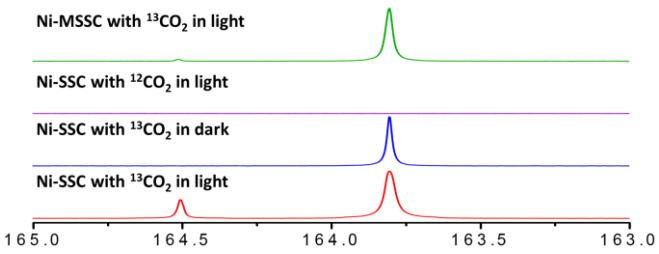

Figure 4. ^{13}C NMR spectra for the product detected in the system of Ni-**SSC** with $^{13}CO_2$ under the light (red line), $^{13}CO_2$ under the dark (blue line) and $^{12}CO_2$ under the light (purple line) and Ni-**MSSC** with $^{13}CO_2$ under the light (green line), respectively.

To further investigate the factors that influence the photo reduction processes, complex Ni-**MSSC** was prepared as a mononuclear nickel complex that represents one corner of the macrocycle Ni-**SSC**. Crystals of Ni-**MSSC** were obtained from slow evaporation of the solution of ligand **MSSC** and $Ni(OAc)_2$. ESI-MS spectrum of Ni-**MSSC** in a DMF solution exhibited an intense peak at m/z = 767.15 (Figure S4). The peak is assigned to the specie of $[Ni(\mathbf{MSSC})_2H]^+$, showing the formation and stability of the complex in solution. Single-crystal structure analysis revealed that the nickel center is affixed to two sulfur atoms and two nitrogen atoms similar to those found for Ni-**SSC**. As was expected, the distances of Ni-S and Ni-N bond

were 2.16 Å and 1.92 Å, same as those in Ni-**SSC**. While the dihedral angles between the pair of the chelating planes were *ca*. 17.0°. Cyclic voltammograms of Ni-**MSSC** recorded in a DMF solution is similar to that of macrocycle Ni-**SSC**. It exhibits a reversible reduction at $E_{1/2}$= −0.87 V vs SCE under argon atmosphere and a new cathodic wave near the potential of Ni^{II}/Ni^{I} is responded to the addition of $\mathbf{Et_3NH^+}$, while no obvious respond toward carbon dioxide was observed (Figure S11). Most likely, the strained coordination of the ligand in Ni-**SSC** results in a more distorted coordination at the Ni centers, which is favourable for the activation of the carbon dioxide reduction.[16]

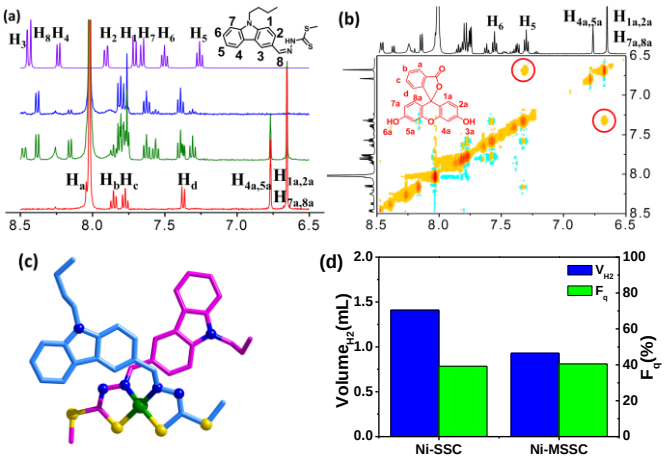

Figure 5. (a) Partial ^{1}H NMR spectrum of ligand **MSSC** (purple line), Ni-**MSSC** (blue line), Ni-**MSSC** with **Fl** (green line) and **Fl** (red line); (b) Partial NOESY of Ni-**MSSC** and **Fl** mixture in DMF, (c) Structure of the molecular Ni-**MSSC** and (d) The volume of hydrogen production and the amount of fluorescence quenching with the same metal moles (45 μM) of Ni-**SSC** and Ni-**MSSC**, respectively.

UV-vis absorption spectra of **Fl** upon the addition of Ni-**MSSC** show an interaction between the two components (Figure S5).The better solubility of Ni-**MSSC** made the ^{1}H NMR investigation on the interaction between the ligand and the **Fl** possible. The ^{1}H NMR spectrum of Ni-**MSSC** (1 mM) in the presence of **Fl** shows significant increase of the signals associated with protons H, showing the close contact between these units which may attributed to the stacking interactions between the aromatic rings of Ni-**MSSC** and **Fl** (Figure 5a).[31] The NOESY spectrum of the solution Ni-**MSSC** (1 mM) and **Fl** (1 mM) shows obvious H-H interactions between phenyl rings of **Fl** ($H_{1a,\ 2a,\ 7a,\ 8a}$) and Ni-**MSSC** (H_5, red cycles) (Figure 5b). These results demonstrate the potential π-π interactions between the phenyl ring of Ni-**MSSC** and **Fl**, and it could be deduced that the host-guest interaction of the abovementioned **Fl**⊂Ni-**SSC** supramolecular system was also mainly stabilized by this noncovalent interactions.

The addition of 45 μM Ni-**MSSC** to the solution of **Fl** (10 μM) quenched approximately 40.5% of the emission intensity of **Fl** (Figure S9). The quenching process was also caused by the possible interactions of the ligands and the PET from the excited state **Fl*** to the redox Ni centers in Ni-**MSSC**. In this condition, considering that the ligand moles in Ni-**MSSC** was two times over Ni-**SSC**, the efficiency of neat PET process in the Ni-**SSC** might be higher than that of Ni-**MSSC** in the photocatalytic system.

Table1. Comparison of structure and features between Ni-**SSC** and Ni-**MSSC**

	Ni-**SSC**	Ni-**MSSC**
Structure of coordination plane		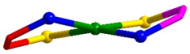
Dihedral angles (°)	23.8	17.0
Redox potential (V)	-0.98	-0.87
V_{H2}(mL)	1.41	0.93
F_q (%)	39.2	40.5
$HCOO^-$ by IC (μmol)	0.46	——
$HCOO^-$ by ^{13}C NMR	obvious	trace

Irradiation of a solution containing **Fl** (4.0 mM), Ni-**MSSC** (30.0 μM), and TEA (10% v:v) in a CH_3CN/H_2O (1:1 in volume) solution at 25°C for 12 h resulted in approximately 0.93 mL hydrogen production, lower than that of the catalyst Ni-**SSC**. Bubbling carbon dioxide to the above mentioned solution, slight $HCOO^-$ anion was detected by the ^{13}C NMR after being irradiated for 12 h, while the amount of $HCOO^-$ was too few to be detected by IC.

Conclusions

In summary, a supramolecular three-membered metal-organic macrocycle for the photocatalytic reduction of protons and CO_2 was reported. It functions by encapsulation of the dye that leads to photoinduced reduction of the nickel complexes. Control experiments using a mononuclear complex that represents one corner of the macrocycle show that this mononuclear complex also quenches the excited state of the dye, but that it leads to less efficient CO_2 conversion. These results reveal that the higher photocatalytic efficiency of the preorganized macrocycle is likely a result of higher activity of the metal complex, caused by the constraint of ligand in the macrocycle Ni-**SSC.** This leads to a more distorted coordination complex of the Ni centers, which is favourable for the activation of the carbon dioxide reduction. In addition, the pseudo-intramolecular electron transfer process attributed to the host-guest complexation is also benefit for the photocatalytic reduction. We therefore conclude that we constructed a new supramolecular artificial photocatalytic system for the reduction of CO_2.

Acknowledgements

We acknowledge the financial support from the National Natural Science Foundation of China (21531001 and 21421005).

Notes and references

1 (a) A. J. Kirby and F. Hollfelder, *From Enzyme Models to Model Enzymes*, RSC Publishing, Cambridge, 2002; (b) J. M. Lehn, *Science*, 2002, **295**, 2400-2403; (c) V. Nanda and R. l. Koder, *Nature Chemistry*, 2010, **2**, 15-24; (d) T. S. Koblenz, J. Wassenaar and J. N. H. Reek, *Chem.Soc. Rev*., 2008, **37**, 247.

2 (a) L. Pauling, *Nature*, 1948, **161**, 707-709; (b) I. Tabushi, *Acc. Chem. Res.*, 1982, **15**, 66-72; (c) D. M. Vriezema, M. C. Aragonès, J. A. A. W. Elemans, J. J. L. M. Cornelissen, A. E. Rowan and R. J. M. Nolte, *Chem. Rev.*, 2005, **105**, 1445-1490;

3 (a) M. Yoshizawa, M. Tamura and M. Fujita, *Science*, 2006, **312**, 251-254; (b) M. D. Oluth, R. G. Bergman and K. N. Raymond, *Science*, 2007, **316**, 85-88; (c) M. L. Singleton, J. H. Reibenspies and M. Y. Darensbourg, *J. Am. Chem. Soc.*, 2010, **132**, 8870-8871.

4 (a) M. Yoshizawa, J. K. Klosterman and M. Fujita, *Angew. Chem. Int. Ed*., 2009, **48**, 3418-3438; (b) T. Murase, S. Horiuchi and M. Fujita, *J. Am. Chem. Soc*., 2010, **132**, 2866-2867; (c) Y. Inokuma, M. Kawano and M. Fujita, *Nature Chemistry*, 2011, **3**, 349-358; (d) K. Ikemoto, Y. Inokuma and M. Fujita, *Angew. Chem. Int. Ed*., 2010, **49**, 5750-5752; (e)Y. Wang, H. X. Lin, L. Chen, S. Y. Ding, Z. C. Lei, D. Y. Liu, X. Y. Cao, H. J. Liang, Y. B. Jiang and Z. Q. Tian, *Chem. Soc. Rev.*, 2014, **43**, 399-411.

5 (a) A. L. Loner, C. Marquez, M. H. Dickman and W. M. Nau, *Angew. Chem. Int. Ed.*, 2011, **50**, 545-548; (b) J. W. Lee, S. Samal, N. Selvapalam, H. J. Kim and K. Kim, *Acc. Chem. Res*., 2003, **36**, 621-630; (c) L. Cronin, *Angew. Chem. Int. Ed.*, 2006, **45**, 3576-3578; (d) C. Schmuck, *Angew. Chem. Int. Ed*., 2007, **46**, 5830-5833.

6 (a) T. Inoue, A. Fujishima, S. Konishi and K. Honda, *Nature*, 1979, **277**, 637-638; (b) S. Sato, T. Arai, T. Morikawa, K. Uemura, T. M. Suzuki, H. Tanaka and T. Kajino, *J. Am. Chem. Soc*., 2011, **133**, 15240-15243; (c) K. Sayama, K. Mukasa, R. Abe, Y. Abe and H. Arakawa, *Chem. Commun*., 2001, **23**, 2416-2417; (d) Y. Sasaki, H. Nemoto, K. Saito and A. Kudo, *J. Phys. Chem. C*, 2009, **113**, 17536-17542.

7 (a) J. Hawecker, J. M. Lehn and R. Ziessel, *J. Chem. Soc. Chem. Comm.*, 1983, **9**, 536-538; (b) Z. Y. Bian, K. Sumi, M. Furue, S. Sato, K. Koike and O. Ishitani, *Inorg. Chem*., 2008, **47**, 10801-10803; (c) M. Kirch, J. M. Lehn and J. P. Sauvage, *Helv Chim Acta*, 1979, **62**, 1345-1384; (d) J. Hawecker, J. M. Lehn and R. Ziessel, *J. Chem. Soc., Chem. Comm*., 1985, **2**, 56-58; (e) R. Ziessel, J. Hawecker and J. M. Lehn, *Helv Chim Acta*, 1986, **69**, 1065-1084;

8 (a) O. K. Varghese, M. Paulose, T. J. LaTempa and C. A. Grimes, *Nano Lett*., 2009, **9**, 731-737; (b) W. Y. Lin and H. Frei, *J. Am. Chem. Soc*., 2005, **127**, 1610-1611; (c) W. Y. Lin, H. X. Han and H. Frei, *J. Phys. Chem. B*, 2004, **108**, 18269-18273; (d) W.Y. Lin and H. Frei, *C. R. Chimie*, 2006, **9**, 207-213; (e) T. W. Woolerton, S. Sheard, E. Reisner, E. Pierce, S. W. Ragsdale and F. A. Armstrong, *J. Am. Chem. Soc*., 2010, **132**, 2132-2133. (f) T.W. Woolerton, S. Sheard, E. Pierce, S.W. Ragsdale and F.A. Armstrong, *Energy Environ. Sci*., 2011, **4**, 2393-2399.

9 (a) M. Raynal, P. Ballester, A. Vidal-Ferran and P. W. N. M. Leeuwen, *Chem. Soc. Rev*., 2014, **43**, 1660-1733; (b) M.Raynal, P. Ballester, A. Vidal-Ferran and P. W. N. M. Leeuwen, *Chem. Soc. Rev*., 2014, **43**, 1734-1787; (c) Y. Murakami, J. Kikuchi, Y. Hisaeda and O. Hayashida, *Chem. Rev.*, 1996, **96**, 721-758; (d) Z. Y. Dong, Q. Luo and J. Q. Liu, *Chem. Soc. Rev.*, 2012, **41**, 7890-7908.

10 (a) R. Chakrabarty, P. S. Mukherjee and P. J. Stang, *Chem. Rev.*, 2011, **111**, 6810-6918; (b) S. Leininger, B. Olenyuk and P. J. Stang, *Chem. Rev*., 2000, **100**, 853-907; (c) S. R. Seidel and P. J. Stang, *Acc. Chem. Res*., 2002, **35**, 972-983; (d) P. J. Stang and B. Olenyuk, *Acc. Chem. Res.*, 1997, **30**, 502-518; (e) N. B. Debata, D. Tripathy and D. K. Chand, *Coord. Chem. Rev*., 2012, **256**, 1831-1945; (f) M. M. J. Smulders, I. A. Riddell, C. Browne and J. R. Nitschke, *Chem. Soc. Rev*., 2013, **42**, 1728-1754; (g) M. J. Wiester, P. A. Ulmann and C. A. Mirkin, *Angew. Chem. Int. Ed*., 2011, **50**, 114-137.

11 (a) C. He, J. Wang, L. Zhao, T. Liu, J. Zhang and C. Y. Duan, *Chem. Commun.*, 2013, **49**, 627-629; (b) X. Jing, C. He, Y. Yang and C. Y. Duan, *J. Am. Chem. Soc*., 2015, **137**, 3967-3974.

12 (a) B. Julien, R. Marc and R. Mathilde, *J. Am. Chem. Soc*., 2014, **136**, 16768-16771; (b) M. Aresta, A. Dibenedetto and A. Angelini, *Chem. Rev*., 2014, **114**, 1709-1742. (c) C. Costentin, M. Robert and J. M. Savéant, *Chem. Soc. Rev*., 2013, **42**, 2423-2436; (d) J. L. Qiao, Y. Y. Liu, F. Hong and J. J. Zhang, *Chem. Soc. Rev*., 2014, **43**, 631-675.

13 (a) B. J. Fisher, R. Eisenberg, *J. Am. Chem. Soc*., 1980, **102**, 7361-7363; (b) J. D. Froehlich and C. P. Kubiak, *J. Am. Chem. Soc.*, 2015, **137**, 3565-3573; (c) M. Beley, J. P. Collin, R. Ruppert and J. P. Sauvage, *J. Am. Chem. Soc.*, 1986, **108**, 7461-7467; (d) J. Schneider, H. Jia, K. Kobiro, D. E. Cabelli, J. T. Muckerman and E. Fujita, *Energy Environ. Sci*., 2012, **5**, 9502-9510

14 E. E. Benson, C. P. Kubiak, A. J. Sathrum and J. M. Smieja, *Chem. Soc. Rev*., 2009, **38**, 89-99.

15 (a) J. Y. Huot and L. Brossard, *Int. J. Hydrogen Energy*, 1987, **12**, 821–830; (b) J. C. Fontecilla-Camps, A. Volbeda, C. Cavazza and Y.Nicolet, *Chem. Rev*., 2007, **107**, 4273–4303; (c) C. Tard and C. J. Pickett, *Chem. Rev*., 2009, **109**, 2245–2274; (d) S. Ogo, R. Kabe, K. Uehara, B. Kure, T. Nishimura, S. C. Menon, R. Harada, S. Fukuzumi, Y. Higuchi, T. Ohhara, T. Tamada and R. Kuroki, *Science*, 2007, **316**, 585–587; (e) B. E. Barton, C. M. Whaley, T. B. Rauchfuss and D. L. Gray, *J. Am. Chem. Soc.*, 2009, **131**, 6942–6943.

16 V. S. Thoi, N. Kornienko, C. G. Margarit, P. D. Yang and C. J. Chang, *J. Am. Chem. Soc*., 2013, **135**, 14413–14424.

17 J. F. Dong, M. Wang, P. Zhang, S. Q. Yang, J. Y. Liu, X. Q. Li and L. C. Sun, *J. Phys. Chem. C*, 2011, **115**, 15089-15096.

18 G. Li, X. Zhou, P. Yang, Y. Jian, T. Deng, H. Shen and Y. Bao, *Tetrahedron Letters*, 2014, **55**, 7054-7059.

19 SMART Data collection software, version 5.629; Bruker AXS Inc.: Madison, WI, 2003. SAINT Data reduction software, version 6.45; Bruker AXS Inc.: Madison, WI, 2003.

20 G. M. Sheldrick, SHELXTL V5.1, Software Reference Manual, Bruker, AXS, Inc.: Madison, WI, 1997.

21 (a) T. Uechi and T. Oniki, *Bull. Chem. Soc. Jpn.*, 1982, **55**, 971-974; (b) T. S. Lobana, P. Kumari, R. Sharma, A. Castineiras, R. J. Butcher, T. Akitsu and Y. Aritake, *Dalton Trans*., 2011, **40**, 3219-3228.

22 (a) A. D. Burrows, R. W. Harrington, M. F. Mahona and S. J. Teat, *CrystEngComm*, 2002, **4**, 539-544; (b) T. S. Lobanaa, P. Kumari, M. Zeller and R. J. Butcher, *Inorg. Chem. Commun*., 2008, **11**, 972-974; (c) N. T. Akinchan and U. Abram, *Acta Cryst*. 2000. **C56**, 549-550.

23 P. Du and E. Richard, *Energy Environ. Sci*., 2012, **5**, 6012-6021.

24 B. Carole, A. Vincent and F. Marc, *Inorg. Chem*., 2007, **46**, 1817-1824.

25 V. S. Thoi and C. J. Chang, *Chem. Commun*., 2011, **47**, 6578-6580.

26 K. A. Connors, Binding Constants, John Wiley, New York, 1987.

27 P. J. Jiang and Z. J. Guo, *Coord. Chem. Rev*., 2004, **248**, 205-229.

28 C. A. Konigstein, *J. Photochem. Photobiol*., 1995, **90**, 141-152.

29 H.Q. Xu, J. H. Hu, D. K. Wang, Z. H. Li, Q. Zhang, Y. Luo, S. H. Yu and H. L. Jiang, *J. Am. Chem. Soc*., 2015, **137**, 13440−13443.

30 H. F. M. Nelissen, M. Kercher, L. D. Cola, M. C. Feiters and R. J. M. Nolte, *Chem. Eur. J*., 2002, **8**, 5407-5414.

31 S. M. Biros, R. M. Yeh and K. N. Raymond, *Angew. Chem. Int. Ed*., 2008, **47**, 6062-6064.